Simulation of Semiflexible Cyclic and Linear Chains Moderately and Strongly Confined in Nanochannels

DATASET *in* MACROMOLECULES · MARCH 2012

Impact Factor: 5.8 · DOI: 10.1021/ma202730c

2 AUTHORS:

Zuzana Benková
Slovak Academy of Sciences
23 PUBLICATIONS **358** CITATIONS
SEE PROFILE

Peter Cifra
Slovak Academy of Sciences
96 PUBLICATIONS **1,025** CITATIONS
SEE PROFILE

Macromolecules

Article

pubs.acs.org/Macromolecules

Simulation of Semiflexible Cyclic and Linear Chains Moderately and Strongly Confined in Nanochannels

Zuzana Benková*[,†,‡] and Peter Cifra[†]

[†]Polymer Institute, Slovak Academy of Sciences, Dúbravská cesta 9, 845 41 Bratislava, Slovakia

[‡]REQUIMTE, Chemistry Department, University of Porto, Rua do Campo Alegre 687, 4169-007 Porto, Portugal

Supporting Information

ABSTRACT: The constraints due to the chain closure in combination with the geometrical constraints of a DNA molecule are inevitable for many biological processes. In this work, structural properties of flexible and semiflexible cyclic chains and their linear analogues confined in cylindrical channels were studied using the coarse-grained Metropolis Monte Carlo simulations. The radius of gyration satisfactorily represents the longitudinal stretching of both chain topologies. Transition between the moderate and strong confinement regime of semiflexible cyclic chains is described for the first time. Qualitatively similar response of the chain elongation to the confinement strength variation $R_g(D)$ is obtained in the case of cyclic chains. However, the relative chain extension is stronger, the Odijk strong confinement regime is extended to larger channel diameters D, and under moderate confinement the chain extension declines less steeply for cyclic chains. All three findings are explained in terms of the strong self-avoidance of confined chains relative to their linear analogues and the last finding is consistent with the reported experimental measurements. In the Odijk regime, the relative chain extension is governed by the same analytical functions provided half of the contour length for a cyclic chain is considered at the full extension. The orientation correlations for a cyclic chain in narrow channels are characterized by a typical sharp central minimum. Upon increasing the channel cross-sectional area, the minimum is broadened, turns into a negative maximum and, ultimately, the orientation correlations merge with those for a free cycle. Confined flexible and less stiff chains resemble their linear analogues more readily. The static structure factor for tightly confined chains provides better differentiation between the chain architecture than for free chains.

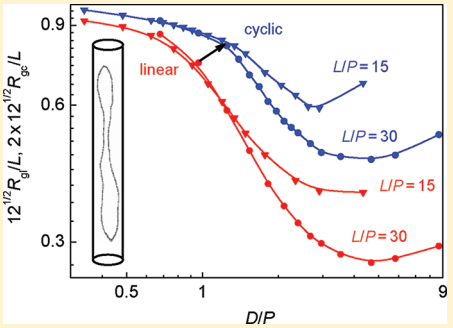

1. INTRODUCTION

In biological systems, biomacromolecules usually adopt conformations perturbed by the constraints invoked by a crowded cellular environment. Because of the reduced conformational freedom, the structure of a confined chain appreciably differs from the structure of a free chain in bulk. Exploring the structural changes triggered by confinement is inevitable for understanding biological properties and functions of DNA and other biomacromolecules as well as for manufacturing nanopores and nanochannels used to investigate and manipulate DNA. The free space achievable for a confined biomacromolecule is usually of micro- or nanoscale dimensions, which often means orders of magnitude smaller dimensions than the unperturbed size of a free biomacromolecule. Depending on the dimensionality of the confining object, classified according to the number of dimensions in which a chain is prevented from relaxation as uni-, bi-, or triaxial geometries (in fully symmetric approximation being slit, channel, or sphere, respectively), the structural and dynamic properties of confined macromolecules are substantially modified.

Recent advances in visualization and manipulation of semiflexible biopolymers in experimental techniques dealing with the macromolecular systems have recorded a great improvement in providing information on single-chain systems. Of special relevance to nanotechnology are the experimental approaches based on the chip-based micro- and nanofluidic devices combined with the florescence microscopy.[1−7] In these experimental setups, the extensions and Brownian dynamics of solvated chains, for example, DNA molecules being very often scrutinized, are affected.

The significant elongation of a DNA molecule was attained at the experimental level in cylindrical nanochannels, as high as 88% of the entirely stretched DNA backbone.[7] The average chain extension dependence on its molecular weight achieved in these experiments are consistent with the blob-theory predictions worked out by de Gennes.[8,9] Accordingly, under the biaxial constraints, a chain is viewed as a linear sequence of self-avoiding impenetrable blobs. The size of a particular blob is equivalent to the diameter of the channel cross-section. A fragment of the chain conforming to each blob obeys statistics of an unconfined chain. Assuming the excluded volume (EV) interactions among segments within each blob, the linear array

Received: December 19, 2011
Revised: February 16, 2012
Published: March 1, 2012

   dx.doi.org/10.1021/ma202730c | *Macromolecules* 2012, 45, 2597−2608

of such a blob determines the average chain extension along the channel axis

$$R \approx L\left(\frac{Pw}{D^2}\right)^{1/3} \quad (1)$$

where L is the contour length of a chain, P and w are its effective persistence length and width, respectively, and D stands for the diameter of a channel. Validity of eq 1 requires a sufficiently long chain comprising enough blobs for good statistics as well as sufficient number of segments in a blob for the EV interactions. The latter condition is controlled by the persistence length and width of the chain backbone (for a given polymer being a function of the ionic strength) and by the diameter of the channel cross-section since $D \approx (gl)^{3/5}(Pw)^{1/5}$, g is a number of segments constituting one blob and l is a bond length between two consecutive segments.

In the context of the channel cross-section dimension, it should be pointed out that the de Gennes moderate-confinement regime is restricted to $P \ll D \ll R_{g0}$; R_{g0} is the radius of gyration of a corresponding free chain. Beyond the upper boundary, a chain retrieves the conformation of a free chain. Once the channel width drops approximately below the Kuhn statistical segment ($2P$), the EV interactions fade away and the conformation of a confined chain is governed by the interplay of the confinement strength and intrinsic chains stiffness. In this strong-confinement regime, a polymer becomes preferentially directed and thus the contour length is stored solely in deflections of a chain from channel boundaries. The new characteristic length scale, the deflection length λ, introduced by Odijk for this regime,[10] scales as $\lambda \approx (D^2P)^{1/3}$ and represents the average distance along the chain contour between two consecutive deflection points. Using these arguments leads to the following relation for the chain extension

$$R = L\left[1 - A\left(\frac{D}{P}\right)^{2/3}\right] \quad (2)$$

where A is a constant dependent solely on the geometry of a cross-section.[11] The transition between the moderate-confinement (de Gennes) regime and the strong-confinement (Odijk) regime occurs at the channel width of the order of the persistence length.[2,12,13] Notice that in both regimes, the chain elongation is linear in the chain contour length as is clear from eqs 1 and 2. This is an advantageous phenomenon in sizing of DNA fragments in nanofluidic arrays.

Experimental measurements gave support to the linear dependence of the chain extension on the chain contour length and point out the importance of this relation in one-to-one mapping between genomic order and measured position along the stretched chains.[1] However, scaling of the chain extension with the strength of moderate confinement $R \sim D^x$ yields the exponent x slightly departing from the predicted value $-2/3$.[2,6] The steeper decrease in chain extension with increasing cross-section dimensions was reported.[2,6] This exponent appeared to be a nonuniversal quantity[6] as a consequence of the transition regime at which the reported experiments were conducted. We found similar scaling relation, performing the Metropolis Monte Carlo (MC) simulations on single linear coarse-grained DNA chains confined in a channel and explained the steeper decrease by the tendency of semiflexible chains to ideality.[13,14] However, the recent mean-field analysis shows that, except for very wide channels, there is no power-law dependence of the axial chain extension on the channel diameter even for the infinitely long chain limit.[15] In agreement with computer simulations and experimental measurements, this analysis predicts rather steeper decay in this regime.[15]

Among the experimental and theoretical works focused on linear chains trapped in a constrained space, special attention is paid to the semiflexible biopolymers such as DNA molecules or actin filaments.[16−19] Nevertheless, in comparison with a relatively great deal of results achieved for biaxially confined linear macromolecules, the number of works aimed at their cyclic analogues is relatively scarce.[6,20,21] This means an inadequate imbalance in regard to the widespread occurrence of prokaryotic genomes and plasmids which are of circular topology and play an important role in manifold biochemical processes.[22] It is the ring topology of biomacromolecules which is essential to many biological and biochemical processes.

In order to shed light into the response of cyclic chains to the biaxial geometrical confinement in addition to the topological circularity constraints, we have carried out simulations using the Metropolis MC method. Since the majority of biopolymers are stiff on the length scale comparable to their persistence length, we have studied flexible as well as semiflexible chains. We have investigated the moderate chain contour length corresponding to a few persistence lengths representing the contour length-persistence length ratio intrinsic to many biopolymers relevant to biological regulatory functions or to a gene therapy based on plasmids. The conformations of closed semiflexible chains induced by the cylindrical constraints were compared with the open chain analogues as well as with the unconfined counterparts in order to address the effects arising from the topological and biaxial geometric constraints. The influence of backbone stiffening was investigated through the comparison with analogous flexible chains.

This study is aimed to fill the gap in investigation of cyclic flexible and semiflexible chains confined in a cylindrical channel and to compare their behavior with corresponding linear counterparts. The response of the chain elongation to the confinement strength is scrutinized and regimes close to the original Odijk and de Gennes regimes are investigated for cyclic macromolecules. The existence, behavior and location of a confinement transition from the weak to strong confinement for cyclic chains are intriguing issues. Under the strong confinement, $D/P < 1$, a linear chain can be trapped fully extended in a narrow channel of the width D almost as small as the chain thickness. The question that emerges is whether a semiflexible cyclic chain with two natural loops stemming from the chain closure can be trapped in such a narrow channel. Apart from the chain extension-confinement strength curves, the orientation correlations and static structure factor are examined as the quantities differentiating both chain architectures.

The rest of the paper is organized as follows. The details of the simulations including the simulation technique, the potential functions and polymer model systems are outlined in the next section. Section 3 divided into four subsections presents the results obtained in this study. In section 4, our main conclusions are summarized based on the results presented in previous discussion.

2. METHODOLOGY

The semiflexible chains were represented by a bead−spring worm-like chain (WLC) model which has been adopted in previous studies of chains threading between inter connected cavities[23] and the structural properties of confined semiflexible polymers.[24,25] This model differs from the classical WLC model in the discretization of the chain backbone into N effective monomers (beads) connected along a chain by the fluctuating effective bonds (springs) of an average length $\langle l \rangle$. Since the bonds were allowed to vibrate around a preferred value, the contour length $L = (N - 1)\langle l \rangle$ in the case of open chains and $L = N\langle l \rangle$ in the case of closed chains underwent small fluctuations.

Molecular simulations were carried out using the Metropolis Monte Carlo technique. The total potential energy of a system was composed of contributions due to the effective bond stretching, nonbonded pair interactions between beads, and bending of two consecutive effective bonds from their collinear arrangement. Since we focused on the behavior associated with the topological effects we truncated detailed local conformation properties for simplicity reasons. In the future refinements especially the torsion rigidity could be included together with the bending rigidity.[26] The role of torsion, however, has not been well established yet. It was shown that at viral packaging the torsion can be omitted from the simulations without alteration of DNA conformation or the free energy of packaging even at low volume fraction or at early stages of filling the bacteriophage.[27] The MC simulations of a DNA molecule confined in a nanochannel using primitive model of DNA which did not consider torsion interactions also produced results in a good agreement with the experimental observations and theoretical prediction.[7] However, for a circular dsDNA chain, the assumption of the neglected torsional effects is adequate only provided it is in a torsionally released, nicked state. In addition, one should not resort to this model in the case the short-range DNA self-interactions, especially dehydration and cholesteric effects are present.

We adopted the established model used previously for bond stretching and nonbonded interactions.[28] The lengths of effective bonds were determined by the finitely extensible, nonlinear elastic potential (FENE)

$$\frac{U_{\mathrm{FENE}}(l)}{k_{\mathrm{B}}T} = -\kappa(l_{\max} - l_{\mathrm{o}})^2 \ln\left[1 - \left(\frac{l - l_{\mathrm{o}}}{l_{\max} - l_{\mathrm{o}}}\right)^2\right] \tag{3}$$

The bond vibrations were considered to be temperature independent with the spring constant $\kappa = 20$. The bond length was restricted to the preferred value $l_0 = 0.7$ and allowed to oscillate by the increment $l_{\max} - l_0 = 0.3$. The maximum allowable bond distance $l_{\max} = 1$ was identified with the length unit.

The nonbonded interactions were characterized by a Morse potential[28] which contains repulsive and attractive terms.

$$U_{\mathrm{M}}(r) = \varepsilon\{\exp[-2\alpha(r - r_{\min})] - 2\exp[-\alpha(r - r_{\min})]\} \tag{4}$$

where the energy at minimum ε, the distance at minimum $r_{\min}$ and the steepness of the potential energy function α were set to 1 $k_{\mathrm{B}}T$, 0.8 and 24, respectively. This combination yields the core radius of a bead $w/2 \approx 0.38$. As the core diameter w exceeded the effective bond length $\langle l \rangle \approx l_0$ by a factor of about 1.08 the utilized approach belonged to partially fused-spheres molecular models in contrast to the tangent sphere model, where $w = \langle l \rangle$. The nonbonded interactions were marginally small for $r > l_{\max}$.

The bending energy was quantified by the bending potential[29]

$$U_{\mathrm{b}}(\gamma) = b^*(1 + \cos\gamma) \tag{5}$$

where γ was the valence angle made by the two consecutive effective bonds. The stiffness of chains was considered to be temperature dependent through the bending parameter $b = b^*/k_BT$ since b^* was proportional to the pair-contact interaction energy ε entering eq 4, $b^* = C\varepsilon$. Except for the bending stiffness of a rod the bending parameter also includes the effect from the nonbonded interactions between chain segments, it leads to the orientation correlation between chains and to the chain stiffening by interactions or by lowering the temperature. Coupling of parameters of the interaction potentials is common in the coarse-grained simulations and allows for a reliable prediction of the polymer−solvent phase diagram.[30] The simulations were performed, however, at constant reduced temperature $T^* = k_{\mathrm{B}}T/\varepsilon = 1$ representing good solvents, since the reduced theta temperature of the model flexible linear chain is at $T_\theta^* = 0.62$. As was shown and explained at theoretical and experimental level,[31] the topological constraints ensuing from the chain closure are responsible for entropy reduction and for increase of the excluded volume effect.[32] This leads to a drop of the T_θ value for circular chains and thus the good solvent conditions used in these simulations apply for cyclic polymers as well.

The investigated closed and open polymers comprised $N = 300$ effective monomers. The bending parameter b introduced in the expression for the bending energy 5 quantified the rigidity of chains. For linear infinitely long WLC chains the elasticity theory of semiflexible rods relates the parameter b directly to the persistence length P, defined as the average projection of the end-to-end vector on the direction of the first bond, through $b = P/\langle l \rangle$. The validity of this relation for the discretized WLC model used in this work was confirmed in previous simulations.[33] This value of persistence length can be extracted from the initial exponential decay of the orientation correlations. Recently, it has become clear that for real polymer chains the standard definition of persistence length as a measure of the local chain stiffness should be modified mainly due to an increased flexibility of chain ends.[34,35] In ring polymers, however, we are in more favorable situation since we do not need to subtract the effect of more flexible chain ends when evaluating the orientation correlations along the chain backbone. In addition to simulations of semiflexible chains of the stiffness $b = 10$ and 20, corresponding to $L/P = 30$ and 15, respectively, we examined fully flexible ($b = 0$) chains.

At this point it is instructive to show the mapping of the presented model to a double stranded DNA chain.[36] First, the bond length l_0 is set equal to the effective diameter $d = 2.5$ nm of a dsDNA chain (notice that the bond length in model is very close to the diameter of a bead core). The commonly accepted persistence length of about $P = 50$ nm, i.e., $P/l_0 = b = 20$, represents the intrinsic stiffness of DNA at physiological conditions. However, this value is length-scale dependent and might not necessarily characterize the true stiffness of a confined DNA chain. Rather it might be altered across cells, cellular states, as well as locally within any given cell depending on its biological state. This type of parametrization of the

dx.doi.org/10.1021/ma202730c | Macromolecules 2012, 45, 2597−2608

coarse-grained bead−spring model was used previously and performed well in describing the extension of linear DNA molecules in channels and of toroidal packing of DNA in viral capsids.[37−39] Comparison of the results obtained with the two different stiffness parameters might supply the effect of increased ionic strength responsible for diminishing of the backbone stiffness.[40,41]

The confinement effect of a channel was modeled through the cylindrical hard-wall potential. The transverse dimension accessible for the bead centers in a channel was characterized by the diameter D^*. However, to consider the space reachable for all the bead volume, the diameter of the channel was assigned as $D = D^* + w$. Such a width for the bead volume was used in other simulation studies of confined polymers.[42,43] Periodic boundary conditions were applied along the channel axis. The lumen of a channel covered the range $D/l_0 = 6.80-86.80$.

For the simulations of linear chains the procedure of the reptation chain updates with 3×10^7 MC cycles of trial moves was used to obtain the ensemble averages. The initial conformations for the simulations were a straight rod and a prolate ellipse aligned with the channel axis, for a linear and for a circular chain, respectively. The conformations of closed chains were generated by small trial random displacements of beads. The amplitude of small displacements (kinks) was 0.125 l_0. In order to prevent circles from opening the quasi-terminal segments 1 and N were excluded from these motions. After a predefined number of kinks, corresponding to the number of chain segments allowed for the random displacement $(N - 2)$, new quasi-terminal segments were selected randomly and the chain was subject to respective renumbering. The number of described MC cycles varied between 2×10^8 to 4×10^8. The equilibrium of the simulated systems was judged from the smoothness of the distribution function of the radius of gyration evaluated from the histograms (Figures S1−S6, Supporting Information). The estimated errors of ensemble averages in the chain extensions were typically within the size of figure symbols.

3. RESULTS AND DISCUSSION

3.1. Chain Extension. It has been well established that a linear chain confined to a sufficiently long and narrow channel is significantly extended along the channel axis. Figure 1 compares the logarithmic plots of the chain extension-channel diameter functions obtained for linear flexible ($b = 0$) and semiflexible ($b = 10, 20$) chains of the length $N = 300$ with their cyclic analogues. Because of the absence of terminal monomers in cyclic chains, the extension is quantified using the radius of gyration

$$R_g = \langle R_g^2 \rangle^{1/2} = \frac{1}{N}\left(\frac{1}{2}\sum_{i=1}^{N}\sum_{j=1}^{N}\langle R_{ij}^2\rangle\right)^{1/2} \quad (6)$$

where R_{ij} denotes the distance between the effective monomers i and j and the angle brackets stand for averaging over all equilibrated chain conformations.

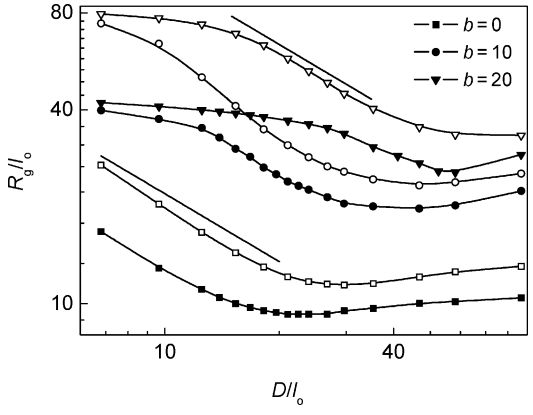

Figure 1. Logarithmic plot of the radius of gyration R_g/l_0 for cyclic (solid symbols) and linear (open symbols) chains of indicated stiffness parameters b as a function of the channel diameter D/l_0. The solid lines illustrate the slope of $1 - 1/\nu = -0.701$ with $\nu = 0.588$.

In Figure 1, the curves for flexible chains of both topologies and of the same contour length are very similar displaying a typical nonmonotonous pattern. Upon reduction of the channel cross-section size, starting from the weak confinement, chains are slightly squeezed and, after a shallow minimum, their radius of gyration follows an increasing trend with further reduction of D under the moderate and strong confinement. The scaling exponents in this linear part are -0.65 ± 0.03 and -0.76 ± 0.02 for cyclic and linear chains, respectively. No evidence for the Odijk regime has been detected for flexible chains of both architectures, in line with the absence of bending energy penalty.

For chains of both topologies and of $b = 10$, the behavior in the weak confinement is akin to that of flexible chains. However, in the narrow channels there is a small curvature found in the plot for a linear chain while the Odijk regime is already recognizable in the plot for a cyclic chain. For both nonzero stiffness parameters the radius of gyration for both chain architectures tends to the same limit as $D \to 0$ (Figure 1). In the moderate-confinement regime, the scaling exponents gained by fitting of the linear section of the curves are -0.69 ± 0.02 and -0.85 ± 0.02, respectively, for cyclic and linear chains of $b = 10$. In fact, the extension-confinement strength function $R_g(D)$ for a chain of the linear topology and of the stiffness $b = 20$ more or less parallels the plot for a cyclic chain of $b = 10$. The linear regime is again characterized by faster decrease for the open chain analogues. The respective exponents are -0.47 ± 0.02 and -0.71 ± 0.01 for cyclic and linear chains of $b = 20$, the former value should be taken only roughly because of a very short interval of the linear part. These findings are qualitatively consistent with the experimental results obtained for circular and linear DNA molecules[6] where the authors reported the corresponding exponents of -0.65 ± 0.01 and -0.85 ± 0.01 for a circular and linear DNA.

In the present simulations, the chain length in the number of segments is below the limit P^3/l_0w^2 roughly corresponding to approximately 850 and 6800 monomers for chains of $b = 10$ and 20, respectively, which is prerequisite for the existence of the classic de Gennes regime for linear chains.[12] In this regime, a chain is represented by an array of the impenetrable isometric blobs with the EV statistics inside each blob. Nevertheless, even the shorter contour length of a chain might be sufficient for the appearance of the de Gennes regime extended toward narrower channels, in which a chain is envisioned as an array of the anisometric blobs each containing $c(D^4P)^{1/3}/l_0w^{2/3}$ monomers obeying Gaussian statistics with a corresponding longitudinal length $(2NPl_o)^{1/2} = (2c)^{1/2}(DP)^{2/3}/w^{1/3}$ (c is a constant of the order of unity).[12] However, the extension of a chain is given by eq 1 in both the isometric and anisometric blob regimes. In the

dx.doi.org/10.1021/ma202730c | Macromolecules 2012, 45, 2597−2608

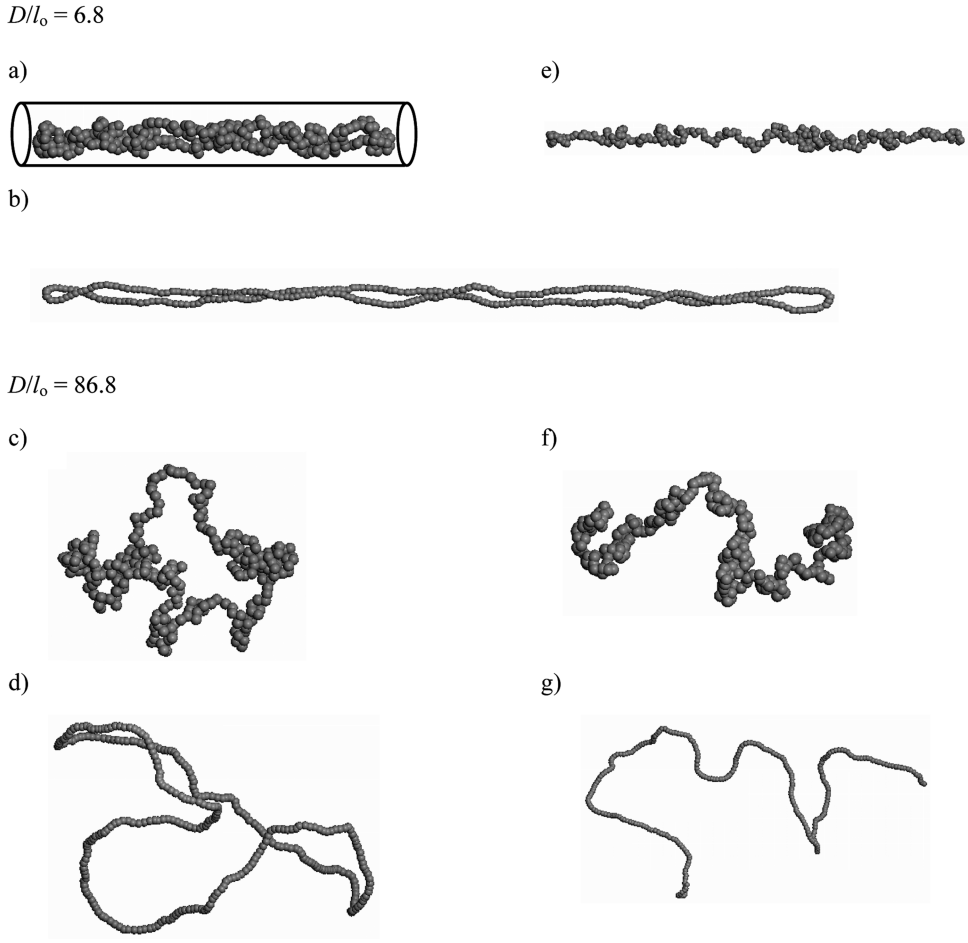

Figure 2. Snapshots illustrating the instantaneous conformations of cyclic (a–d) and linear chains (e–g) confined to a cylindrical channel of indicated diameter D/l_0. Snapshots a, c, e, f depict flexible chains ($b = 0$) and snapshots b, d, and g depict semiflexible chains ($b = 20$). The real size of the effective monomers is assumed to be the same in all snapshots.

later regime assuming $c = 1$, from 2 ($b = 20$, $D/l_0 = 20$) to 7 ($b = 10$, $D/l_0 = 10$) anisometric blobs can be formed within investigated chains of the length $N = 300$ monomers. For comparison, in the experimental study on linear (48.5 kbp) and circular (42.2 kbp) DNA[6] using the persistence length of 50 nm and the effective width of 2.5 nm the contour lengths of the investigated chain backbones were amenable to accommodate only about 5 to 18 anisometric blobs in channels of the geometrically averaged diameter of about 240 and 97 nm, respectively, however the chains were too short for even one isometric blob.

The slightly less pronounced decreasing tendency of the axial extension with the increasing channel width for a cyclic chain when compared with the extension of a linear analogue might be explained in terms of the chain extension dependence on the channel diameter scaling as $D^{1-(1/\nu)}$, where ν is the Flory exponent. As has been highlighted by the direct renormalization theory[44] and confirmed at the experimental level[45] the constraints due to the chain closure do not affect the Flory exponent for a free chain. However, in Figure 1 the scaling in the region of moderate confinement suggests a larger effective value of ν for cyclic chains ($\nu_c = 0.592 \pm 0.013$ vs $\nu_l = 0.541 \pm 0.036$ for $b = 10$). This discrepancy might be attributed to a more compact organization of monomers in a cyclic chain under the biaxial confinement caused by the doubled appearance of the monomers along the channel axis within the closed backbone. The denser segment arrangement follows also from the pattern of the structure factor-wavevector dependence discussed below. Consequently, monomers of a cyclic chain are slightly more susceptible to self-avoidance under the confinement and the effectively higher Flory exponent for the cyclic polymers diminishes the absolute value of exponent $x < 0$ in the D^x-dependent extension. Similar interpretation has been already offered by the experiments of Persson et al.[6] The same effect was observed also for linear chains.[46] Partly folded DNA chains confined in nanochannels were reported to have the extension of folded fragments greater by 30% as opposed to unfolded fragments. This was attributed to a greater self-exclusion in these folded fragments induced by a channel.

The deviation from the predicted $R_g(D)$ dependence of the chain extension is most likely due to the short-range of the extended de Gennes regime and thus due to a relatively large contamination ensuing from the intermediate regime between the Odijk regime and the de Gennes regime.[12] The range of the de Gennes regime becomes even shorter for cyclic chains because of the more striking apparent stiffening induced by the geometrical and topological constraints, which expands the Odijk regime toward larger channels. In order to achieve the quantitative agreement with the theoretically predicted $x = -0.701$ for $\nu = 0.588$, as well as to discern all predicted regimes,[12] one should rather resort to much longer chains,

dx.doi.org/10.1021/ma202730c | *Macromolecules* 2012, 45, 2597–2608

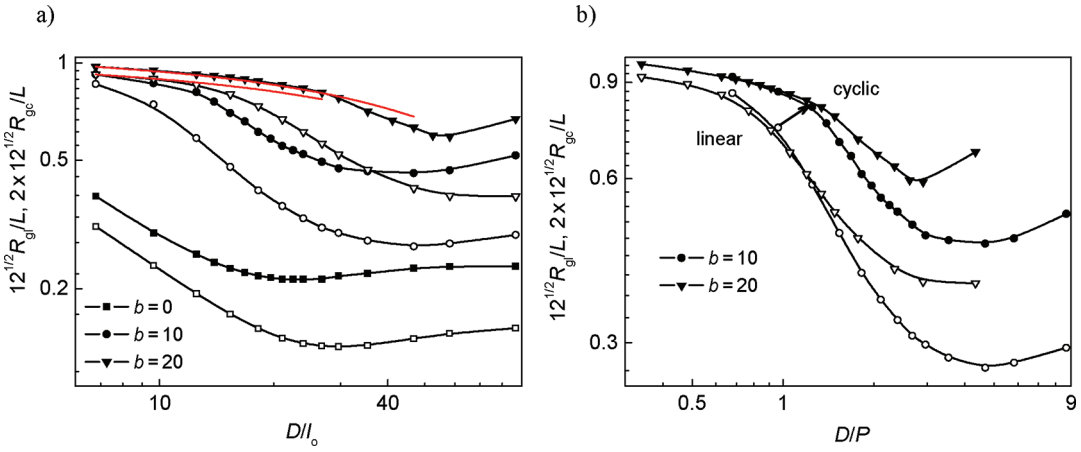

Figure 3. Logarithmic plot of the radius of gyration R_g reduced by the corresponding maximal feasible extension $L/(2\sqrt{12})$ and $L/\sqrt{12}$ for cyclic (solid symbols) and linear chains (open symbols), respectively, as a function of the channel diameter D/l_0 (a) and D/P (b). Stiffness parameters b are indicated in the legend. The solid lines in part a are fits based on eq 7.

which is beyond the scope of the present study. Considering the length and width of commonly used DNA molecules in experimental studies of confinement effects, it appears to be difficult to achieve the de Gennes regime for semiflexible chains even at the experimental level.[2,6]

The snapshots in Figure 2 outline the instantaneous conformations of flexible and semiflexible, open and closed chains trapped in a channel of $D < P$ as well as in a channel of $D > 2R_{g0}$.

In order to compare the relative extension of cyclic and linear chains the plots of the radius of gyrations reduced by the maximal achievable extension, being $L/\sqrt{12}$ for a linear chain and $L/(2\sqrt{12})$ for a cyclic chain, are presented in Figure 3a. These plots confirm the enhanced tendency of closed chains to the elongation in a biaxially confined space. Especially, in the weak and moderate confinement regimes (not too small D), the relative elongation of cyclic chains non-negligibly exceeds the relative elongation of linear chains. Since the circular chain architecture imposes back folding of a chain at both extreme positions of monomers in a channel, the monomers become more prevented from local back folding. In order to release the overcrowding caused by the enhanced monomer density, a cyclic chain becomes stretched along the channel axis. In very narrow channels the difference in the relative extension between semiflexible chains of both architectures diminishes as the plots approach unity, i.e., the limit value of reduced R_g characteristic for the maximally extended conformations.

On the contrary, the plots for flexible chains are getting closer in relative extension as the confinement strength increases but are still far from being merged. Since there is no correlation between monomers along the flexible chain backbone arising from bending interactions, the conformation is dictated exclusively by the EV interactions. Thus, in the case of flexible chains, one might expect a great deal of the chain extension in channels of the diameter comparable to the two effective widths of the monomer segments, i.e., $\sim 2.18l_0$. However, as the simulations revealed, even in such a narrow channel the ratio of $2\sqrt{12}R_g/L = 0.80$ and $\sqrt{12}R_g/L = 0.73$ for a cyclic and linear chain, respectively, is still less than unity approaching by semiflexible chains (Figure 3a). This finding along with the absence of the Odijk regime for flexible chains are evidence for presence of the coiled backbone sections instead of the locally stiff segments bouncing against channel walls.

Figure 3a also involves an analogue of eq 2 for the relative elongation of chains of both architectures and of the stiffness $b = 20$. Though this equation is derived for the longitudinal end-to-end distance, one may see that it applies to the radius of gyration as well. What is more striking, it applies also to cyclic chains and one might use the following equation in the analysis of cyclic chains in microfluidic devices

$$R_{gc} = \frac{L}{2\sqrt{12}}\left[1 - A\left(\frac{D}{P}\right)^{2/3}\right] \tag{7}$$

Only A parameter was fitted using eq 7, while the value of the persistence length was kept fixed at the value determined by the stiffness parameter b. The fitting procedure yields $A = 0.21$ and 0.20 for a cyclic and linear chain, respectively; both values are virtually equal within the error bar. These estimates are slightly higher than the estimate 0.1701 obtained by simulations for a channel with the cylindrical cross-section[11,47] and agree very well with the prefactor of 0.2 derived analytically when the confinement effect was represented by a parabolic potential.[48] While for a linear chain of $b = 20$ the onset of the Odijk regime might be assigned for a channel of the diameter around $12.51l_0$, the topological constraints due to the circularity shift this value to $D \approx 29.66l_0$. This statement is well supported by the plot of the reduced radius of gyration against the channel diameter reduced by the persistence length D/P (Figure 3b). According to eqs 2 and 7, such plots are anticipated to collapse onto one master curve in the Odijk regime. A satisfactory single curve is obtained for cyclic chains in this region, while for linear chains the coalescence is more shifted to the moderate-confinement regime. However, the expansion of the Odijk regime for cycles beyond $D/P = 1$, characteristic for linear chains, up to $D/P \approx 1.5$ is clearly seen. This is in line with the above discussion of the enhanced local density of monomers caused by the closed chain topology. The strong confinement regime becomes thus wider for semiflexible cyclic chains than for their linear counterparts.

dx.doi.org/10.1021/ma202730c | *Macromolecules* 2012, 45, 2597–2608

The relative mean square extension of a worm-like chain under a strong confinement is often described by the following relation[16]

$$\frac{\langle R^2\rangle}{L^2} = 1 - \frac{\lambda}{2P}\left\{1 + \frac{\lambda^2}{L^2}\left[1 - \sqrt{2}\,e^{-L/\lambda}\sin\left(\frac{L}{\lambda} + \frac{\pi}{4}\right)\right]\right\} \quad (8)$$

from which one may extract λ, or alternatively, the geometry-dependent prefactor a in relation $\lambda = aD^{2/3}P^{1/3}$ when plotted the relative chain extension against D. We have applied this relation to fit $\langle R_g\rangle^2/(12L^2)$ in Figure 4. The half circumference

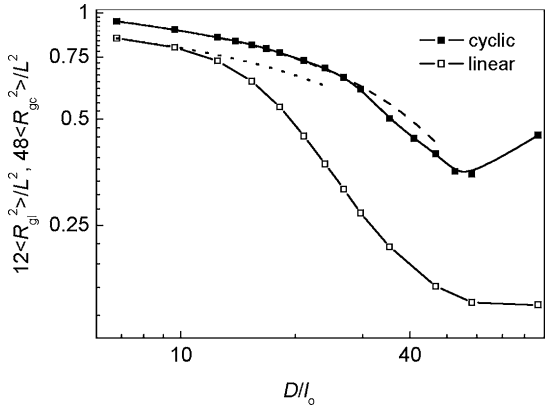

Figure 4. Logarithmic plot of the square radius of gyration R_g^2 reduced by the corresponding maximal feasible square extension $L^2/48$ and $L^2/12$ for cyclic (solid symbols) and linear (open symbols) chains, respectively, as a function of the channel diameter D/l_0. The stiffness parameter is $b = 20$. The dashed and dotted lines are the corresponding fits to eq 8.

length $L/2$ for the contour length of a cyclic chain was used in this relation. These plots are shown in Figure 4 along with their respective best fits which render the numerical prefactor $a = 0.69$. This value agrees fairly well with the value of 0.68 obtained by a two-parameter fit of the orientation correlation data for a linear chain of $b = 20$ to the prediction derived for a worm-like chain model similar to eq 8.[36] Köster et al. obtained the value of 0.76 by fitting the MC results using the same procedure.[49] The difference is most likely caused by the parabolic potential used to mimic the interactions between a chain and a channel wall in ref 49 while hard-wall potential was used in the present study. Nevertheless, our estimate is within the experimental bar of values 0.65−0.8.[49]

3.2. Radius of Gyration to Hydrodynamic Radius Ratio. An important quantity differentiating the ring conformation from the open-chain conformation is the radius of gyration to the hydrodynamic radius ratio R_g/R_h. The hydrodynamic radius was calculated as follows

$$\langle R_h\rangle = N^2\left(2\sum_{i=1}^{N}\sum_{j>i}^{N}\langle R_{ij}^{-1}\rangle\right)^{-1} \quad (9)$$

For free flexible cyclic and linear Gaussian chains, respectively, these analytic values read $(\pi/2)^{1/2}$ and $8/(3\pi^{1/2})$.[32] The excluded volume effects are accounted for through the cluster expansions.[32] The evolution of R_g/R_h ratio with the confinement strength is displayed in Figure 5. The theoretical predictions for free flexible Gaussian chains are also included.

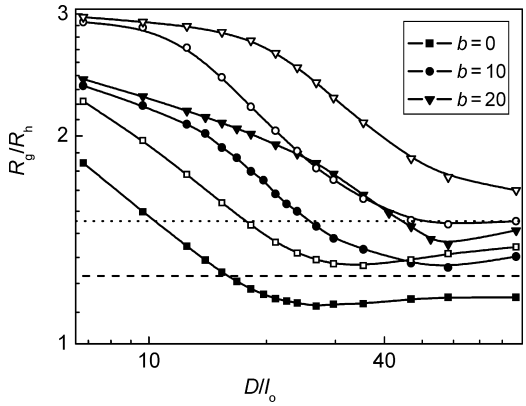

Figure 5. Logarithmic plot of the radius of gyration to the hydrodynamic radius ratio R_g/R_h for cyclic (solid symbols) and linear (open symbols) chains of indicated stiffness parameters b as a function of the channel diameter D/l_0. The dashed and dotted lines, respectively, depict the analytical predictions of $(\pi/2)^{1/2}$ and $8/(3\pi^{1/2})$ for flexible cyclic and linear Gaussian chains.

One should take into account that the results presented in Figure 5 contain contributions due to the EV, local chain stiffness, geometrical and in the case of cyclic chains also topological constraints. Moreover, the chain length is far from the saturation limit where the finite-chain-length correction for both R_g and R_h is negligible. Since the accurate estimation of the hydrodynamic radius is more sensitive to the finite chain length than the radius of gyration,[50] this correction is supposed not to be canceled in the R_g/R_h ratio. To determine the exact value computationally is a challenging task.

As is seen in Figure 5, the R_g/R_h ratio for semiflexible chains of both investigated stiffness parameters tends to the same value in a very strong confinement. This limit is larger for linear chains. In intermediate channels the stiffer chains exhibit larger R_g/R_h ratio. In the case of flexible chains the curves for both chain architectures are more or less parallel. The trend in the plots is qualitatively akin to the trend of corresponding R_g plots (Figure 1) but the shallow minima are slightly shifted toward the larger channel diameters.

3.3. Orientation Correlation Function. Now, we continue this study by investigation of the orientation correlation function $\langle \boldsymbol{u}_i\boldsymbol{u}_j\rangle = \langle\cos\theta_{ij}\rangle = \exp[(-|i-j|\langle l\rangle)/P]$, where $\boldsymbol{u}_i$ and $\boldsymbol{u}_j$ hold for the unit vectors tangent to the chain contour at positions of the ith and jth segments, respectively, θ_{ij} is the angle formed by these vectors and the exponential terms is the WLC representation of the orientation correlations. The averaging runs over all equilibrated MC steps and all pairs of indices i and j separated along the chain backbone by the same section $|i-j|\langle l\rangle$ of the contour length L. This property is applicable to distinguish a cyclic chain from its linear analogue.

The orientation correlations as a function of the segment separation for flexible and semiflexible closed chains of $b = 10$ and 20 confined in channels of different cross-sectional diameters are compared with the respective functions for open counterparts in Figure 6. In the orientation correlations, the closed topology manifests itself by a fundamental difference which is the symmetric shape around $n = N/2$ with a negative minimum, or a negative local maximum in the center of the chain backbone discussed in more detail below.

For a linear chain the deflection from a channel wall demonstrates itself by the local minimum followed by the horizontal line.[36,49] The reduced $\langle \boldsymbol{u}_i\boldsymbol{u}_j\rangle$ value around the

dx.doi.org/10.1021/ma202730c | Macromolecules 2012, 45, 2597−2608

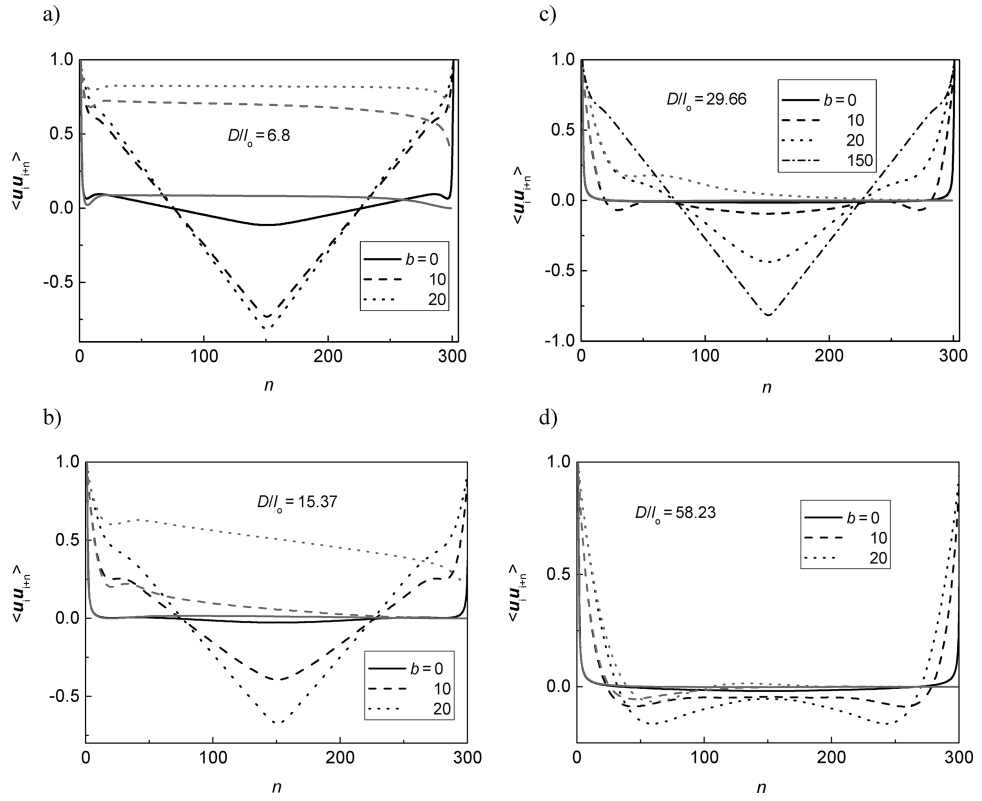

Figure 6. Dependence of the orientation correlations $\langle u_i u_j \rangle$ on the segment separation n along the chain backbone for cyclic (black lines) and linear (gray lines) chains of indicated stiffness parameters b confined in a cylindrical channel of diameter D/l_0 = 6.80 (a), 15.37 (b), 29.68 (c), and 58.23 (d).

deflection point for semiflexible cyclic chains with respect to their linear counterparts implies that the first collision of the cyclic chain backbone with a channel wall is realized at slightly larger angle for closed than for open chains (Figure 6a). This is brought about by a U-turn at the end of a stretched cyclic chain in a channel. The initial decay turns out to be identical for both architectures of a free chain[51] or moderately confined and not too stiff chains (Figure 6b–d). After the initial decay of $\langle u_i u_j \rangle$ followed by a less steeply declining part (Figure 6a, b = 10, 20; Figure 6b,c, b = 20) or a plateau after the local minimum (Figure 6b,c, b = 10) in narrow channels, the plots of the orientation correlations of closed semiflexible chains decrease in a linear fashion toward the central sharp minimum, representing the U-turn, while open chains are characterized by only slightly decreasing orientation correlations. Such a linear behavior of the orientation correlations is a compromise between the correlations of monomers induced by the geometrical and topological constraints combined with the local rigidity of semiflexible cyclic chains. Interestingly, similar pattern of the initial decay of the orientation correlation functions consisting of two regimes has been found for two-dimensional polymer rings in the Langevin dynamics study and confirmed by the experimental measurements.[52] For a flexible chain no plateau evolves and in very narrow channels the linear decrease follows immediately after the local minimum (Figure 6a) in the first half of x abscissa. In wider channels, the orientation correlations for a flexible chain of both architectures are more or less identical, except for the tailing part of the orientation correlations (Figure 6b–d). This implies that the excluded volume and local correlations are more important than the circularity constraint.

While the difference in the orientation correlations appears to be marginal between semiflexible cyclic chains of both b values in the channel of D/l_0 = 6.80 (Figure 6a), the orientation correlations for a flexible chain decrease more slowly in the linear part, since the topological constraints are less severe. As the channel is widened the orientation correlations of a stiffer cyclic chain (b = 20) are getting steeper and deeper around the central minimum than those of a chain of b = 10 (Figure 6b) and thus the differentiation between cyclic chains of different stiffness becomes more pronounced. On the other hand, the channel widening is accompanied by attenuating differences in the orientation correlations between cyclic and linear chains. This trend, however, is least noticeable for a chain of b = 20 (Figure 6c).

Interestingly, in a wide channel of $D/l_0 \approx 60$ a local maximum replaces a central minimum for chains of b = 10 and 20. The shape of the orientation correlations for investigated semiflexible cyclic chains confined in the channel of D/l_0 = 58.23 might be interpreted in terms of loop formation (Figure 6d). Generation of such locked entities is expected for a certain combination of the chain persistence length and channel diameter ratio[53] analogously to the hairpin formation found along the biaxially confined linear chain backbone.[36] The similar orientation correlations were obtained in MC simulations of semiflexible cyclic chains in a confinement of spherical symmetry.[54] After the first collision of a linear chain with the channel wall the oscillations of the chain backbone along the wall is feasible. Averaging of these oscillations over all equilibrated chain conformations damps their amplitudes and ultimately leads to a plateau followed by declining tailing part or, in wider channels, it decreases without any flat region.[15,55,56]

dx.doi.org/10.1021/ma202730c | Macromolecules 2012, 45, 2597–2608

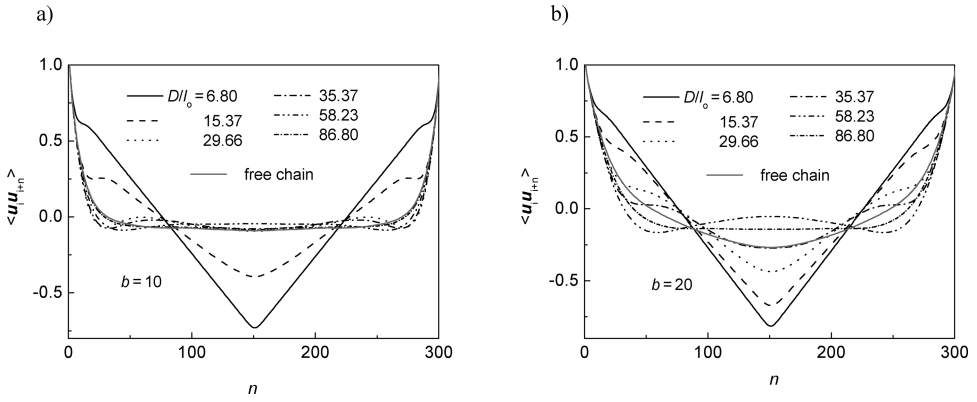

Figure 7. Dependence of the orientation correlations $\langle u_i u_j \rangle$ on the segment separation n along the chain backbone for cyclic chains of the stiffness parameter b = 10 (a) and 20 (b) confined in a cylindrical channel of indicated diameters D/l_0. For comparative purposes, the orientation correlation function of a free chain is also comprised for both stiffness parameters.

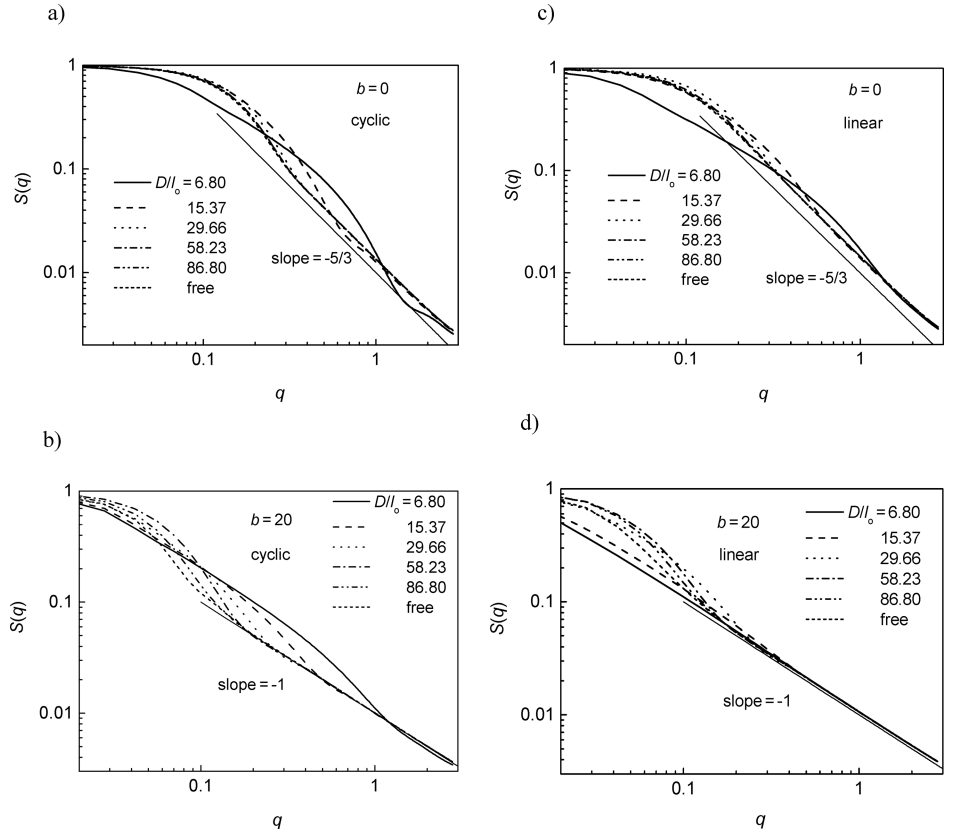

Figure 8. Logarithmic plot of the static structure factor $S(q)$ vs the wavevector q for cyclic (a, b) and linear (c, d) chains of the stiffness parameter b = 0 (a, c) and b = 20 (b, d) in the channel of indicated diameters D/l_0. The plot for a corresponding free chain is also included and the solid straight line in each graph is a guide for the eye representing the slope of −5/3 (a, c) and −1 (b, d), i.e., $q^{-1/\nu}$ type of behavior discussed in the text for the coil and rod-like regime, respectively.

Parts a and b of Figure 7 provide the evolution of the orientation correlation functions with the channel dimensions for a cyclic chain of b = 10 and 20, respectively. Increase of the channel diameter is reflected on the gradual plateau formation between the initially decaying part and linear part of the plot. As mentioned above, in the case of a semiflexible chain of b = 10 the plateau is preceded by a local minimum. Upon channel widening the linear part of the orientation correlation function is simultaneously shortened and reduced in the steepness which shifts the minimum upward along the y axis. As aforementioned, in the channel of D/l_0 = 58.23, the central minimum turns to a local maximum for semiflexible cyclic chains of both stiffness parameters. In the channel of $D > 2R_{g0}$, the geometrical constraints are less important and the orientation correlation functions tend to those of free cyclic chains, faster for more flexible chains. Comparison between orientation correlations for chains of b = 10 and 20 (Figure 7a vs 7b) shows that the orientation behavior of both chains follows the same trend but more flexible chains undergo the particular changes in spacial organization already at stronger confinement. To demonstrate this observation, the orientation correlations for a cycle of b = 150 is added in Figure 6c as well.

dx.doi.org/10.1021/ma202730c | *Macromolecules* 2012, 45, 2597−2608

Worth noting is that the orientation correlation functions for both semiflexible chains confined in channels of various diameters conforming to the Odijk regime intersect in the same narrow region symmetrically distributed around $N/2$. At these points, being $n = 75$ and 226, the orientation correlations essentially attain zero value. The orientation correlations of free semiflexible up to very stiff cyclic chains of the length $N = 300$ were shown to cross each other exactly at these points.[51] As one can see in Figure 2a−d, the restricted space along with the topological constraints is responsible for the enhanced formation of loops. The looping structures are prerequisite to many important biological processes involved, e.g., in the genome-wide coordination of gene expression.[57] Nevertheless, as inferred from the missing regular oscillations in the orientation correlations (Figures 6 and 7) the loops do not possess any defined size upon biaxial confinement as opposed to the oscillatory orientation correlations behavior found for a triaxial confinement using the MC bond-fluctuation model.[58] The authors of this study calculated also the orientation correlations for cyclic chains trapped in the rectangular confinement of a squared base and of a width-to-height ratio 1:8.[58] For the shortest chain they obtained results similar to ours with no central maximum. In other simulation studies, the toroidal structure of a semiflexible chain confined to a spherical cavity produced regular oscillations in the orientation correlations.[59] In other two-dimensional MC study of a linear semiflexible chain exposed to a square confinement, the orientation correlations of the spiral chain conformation possess a similar trend.[60] Since the chain investigated in the present study is free to relax in the longitudinal directions of a channel the same applies to its loops.

3.4. Static Structure Factor. The other quantity which might provide information on polymer topology and conformation is the single-chain static structure factor $S(q)$ plotted against the wavevector q

$$S(q) = \frac{1}{N^2}\left\langle \sum_{i=1}^{N}\sum_{j=1}^{N} \sin(qR_{ij})/qR_{ij} \right\rangle \tag{10}$$

This quantity is accessible through experimental measurements exploiting neutron and light scattering techniques. The behavior of a chain on different length scales is reflected on the behavior of the single-chain static structure factor. The most coarse-grained length scale, the Guinier regime, at $q \ll 1/R_g$ contains only information on the size of a chain. The length scales of the coil and rod regimes, in turn, correspond to the wavevector intervals $1/R_g \ll q \ll 1/P$ and $q \gg 1/P$, respectively. In both regimes, the structure factor is a power-law function of the wavevector $S(q) \sim q^{-1/\nu}$.

The effect of channel diameter on the structure factor for flexible and semiflexible chains of closed and open topology is seen in Figure 8. The behavior of $S(q)$ for a flexible cyclic chain confined in the channel of diameter down to $21.09l_0$ (not shown) is identical with that for a free flexible cyclic chain (Figure 8a). The peculiarity discerning a cyclic chain from its linear analogue is the "hump" pattern in $S(q)$ plot after the Guinier regime. Because of the increased compactness of monomers originating from the tight arrangement of two strands of a cyclic chain along a narrow channel this "hump" becomes even more apparent and consequently the coil regime with the characteristic exponent −5/3 is identified only for a flexible cyclic chain in channels of $D/l_0 \geq 12.51$. In contrast to a flexible cyclic chain, the coil regime in the $S(q)$ plot for a flexible linear chain, though shortened, remains also in very narrow channels (Figure 8c). In wider channels the $S(q)$ for both chain architectures become very similar and one should rather employ the Kratky representation of $S(q)$ to discern between both architectures.[51]

The coil regime is completely suppressed in Figure 8b,d illustrating the structure factor for confined semiflexible cyclic and linear chains of $b = 20$. Such a behavior is expectable on the basis of the enhanced backbone rigidity when the condition $R_g \gg P$ is not met. Similarly to a flexible cyclic chain, the "hump", though less noticeable, occurs also in the $S(q)$ plot for a strongly confined semiflexible cyclic chain (Figure 8b). In very narrow channels, it is the straight line stipulating the rod regime and covering whole interval of the q values for a semiflexible linear chain (Figure 8d) which discerns between both chain topologies. One can infer from Figure 8b,d that on smaller length scales, the impact of confinement on the structure of a confined semiflexible cyclic chain is more substantial when compared with the impact on a confined linear counterpart.

Shown in Figure 9 is the structure factor for a cyclic chain of different stiffness parameters contained in the channel of D/l_o = 29.66. Even for a very stiff cyclic chain of $b = 150$ ($L/P = 2$, $D/P = 0.2$) the typical gradually ceasing oscillations of $S(q)$ found for an unconfined chain of this stiffness[51] are vanishing under strong confinement and only a small sign of the periodic behavior is preserved for such a stiff chain in the channel of $D/l_o = 29.66$. This is expected since the periodicity of $S(q)$ indicates a rigid-ring conformation.

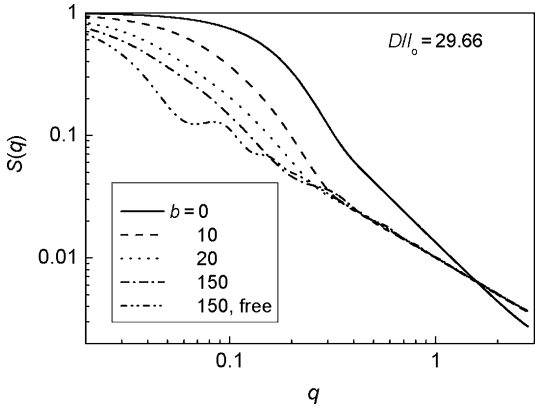

Figure 9. Logarithmic plot of the static structure factor $S(q)$ vs the wavevector q for cyclic chains of indicated stiffness parameters b in the channel of diameter $D/l_0 = 29.66$.

4. CONCLUSIONS

The significance of a circular DNA molecule in constrained spaces encountered in plenty of biological and biophysical phenomena is well-known. However, only a little attention has been paid to such systems so far. Inspired by the experimental measurements conducted on a circular DNA molecule in a tapered nanochannel leading to intriguing confrontation with a linear analogue,[6] we performed the Metropolis Monte Carlo simulations of biaxially confined flexible and semiflexible cyclic chains and their linear analogues. Semiflexible chains of two stiffness parameters corresponding to the ratio $L/P \approx N/b$ of 15 and 30 were investigated.

dx.doi.org/10.1021/ma202730c | Macromolecules 2012, 45, 2597−2608

The chain extension-channel diameter functions for both chain architectures exhibit a qualitative concordance. Nevertheless, the relative extension of cyclic chains is larger than that of linear chains. Under confinement, the densification of segment organization within the closed chains on the intermediate length scale is capable of larger repulsion which effectively raises the Flory exponent ν with respect to linear chains. Thus, the extension-confinement function $R_g \sim D^x$ in the de Gennes regime renders exponent $x = 1 - 1/\nu$ in absolute values lower for cyclic chains and we arrive at the same conclusion as reported in the experimental study.[6] The disagreement with the theoretical prediction of x is ascribed to the short interval of the de Gennes regime, mainly for cyclic chains, and to the stronger self-avoidance in cycles. Because of the stronger self-avoidance of the cycle in a channel its relative extension is enhanced and the Odijk-like strong confinement regime appears already at a weaker confinement $D/P \approx 1.5$ compared to the linear chain where the respective onset is at $D/P \approx 1$.

The Odijk theory for strong biaxial confinement seems to work not only for linear chains and the end-to-end distance but also for cyclic chains assuming the radius of gyration with respect to the halved and whole radius of gyration of a rigid rod for cyclic and linear chains, respectively, as a measure of the relative chain extension. Despite some doubts about existence of the Odijk regime for macrocycles, emerging because semiflexible closed chains can not be stretched to their full contour lengths as linear chains do in narrow channels, it was shown that this approach applies also to cycles. A qualitatively very similar trend in the mean chain extension vs the confinement strength is achieved for the radius of gyration to the hydrodynamic radius ratio, a property characterizing polymer topology and connecting static and dynamic quantity.

In order to pinpoint the difference between chains of both investigated architectures the orientation correlation function and static structure factor are also analyzed.

The symmetric shape around $N/2$th segment in the orientation correlations plotted against the segment contour position along with the negative values around this point found for free cycles remain as the principal discerning features also in constraining space. Besides, however, geometrical constraints combined with the translational invariance (cyclic topology) are reflected also on the shape of the orientation correlations which is now the interplay of the EV effect, conformational entropy, and bending energy (semiflexible chains). The strong confinement gives rise to orientation correlations with a sharp minimum in the middle. This global minimum is broadened upon releasing the confinement strength and before the behavior of the orientation correlations starts reminding the correlations of a free semiflexible cyclic chain it evolves into a broad maximum. This maximum and the two minima are explained by the formation of a locked single loop conformation. A deeper analysis is needed to shed light into this phenomenon which is beyond the scope of the present study.

The logarithmic plot of the structure factor vs the wavevector resolves better the topology of semiflexible chains confined in narrow channels than the topology of free or more loosely confined chains. The oscillations characterizing a stiff ring conformation are suppressed upon the confinement.

The differences in static properties between chains of the closed and open architectures signify interesting comparison of dynamical behavior between both chain architectures. Such information is crucial for comprehension of dynamical processes in biological systems. Therefore, our next focus is on the molecular dynamics simulations of dynamical properties of cyclic vs linear chains of various stiffness parameters.

■ ASSOCIATED CONTENT

Supporting Information

Distribution functions of the radius of gyration (Figures S1−S6) evaluated from the histograms for cyclic and linear chains of the stiffness parameter. This material is available free of charge via the Internet at http://pubs.acs.org.

■ AUTHOR INFORMATION

Corresponding Author

*E-mail: upolzben@savba.sk.

Notes

The authors declare no competing financial interest.

■ ACKNOWLEDGMENTS

This work was supported by the FCT postdoc Grant SFRH/BPD/63568/2009 cofinanced by the European Social Found and VEGA Grant 2/0093/12.

■ REFERENCES

(1) Tegenfeldt, J. O.; Prinz, C.; Cao, H.; Chou, S.; Reisner, W. W.; Riehn, R.; Wang, Y. M.; Cox, E. C.; Sturm, J. C.; Silberzan, P.; Austin, R. H. *Proc. Natl. Acad. Sci. U.S.A.* **2004**, *101*, 10979−10983.

(2) Reisner, W.; Morton, K. J.; Riehn, R.; Wang, Y. M.; Yu, Z.; Rosen, M.; Sturm, J. C.; Chou, S. Y.; Frey, E.; Austin, R. H. *Phys. Rev. Lett.* **2005**, *94*, 196101.

(3) Choi, M. C.; Santangelo, C. D.; Pelletier, O.; Kim, J. H.; Kwon, S. Y.; Wen, Z.; Li, Y.; Pincus, P. A.; Safinya, C. R.; Kim, M. W. *Macromolecules* **2005**, *38*, 9882−9884.

(4) Jo, K.; Dhingra, D. M.; Odijk, T.; de Pablo, J. J.; Graham, M. D.; Runnheim, R.; Forrest, D.; Schwartz, D. C. *Proc. Natl. Acad. Sci. U.S.A.* **2007**, *104*, 2673−2678.

(5) Reisner, W.; Beech, J. P.; Larsen, N. B.; Flyvbjerg, H.; Kristensen, A.; Tegenfeldt, J. O. *Phys. Rev. Lett.* **2007**, *99*, 058302.

(6) Persson, F.; Utko, P.; Reisner, W.; Larsen, N. B.; Kristensen, A. *Nano Lett.* **2009**, *9*, 1382−1385.

(7) Kim, Y.; Kim, K. S.; Kounovsky, K. L.; Chang, R.; Jung, G. Y.; de Pablo, J. J.; Jo, K.; Schwartz, D. C. *Lab Chip* **2011**, *11*, 1721−1729.

(8) de Gennes, P.-G. *Scaling Concepts in Polymer Physics*; Cornell University: Ithaca, NY, 1979.

(9) Brochard-Wyart, F.; Tanaka, T.; Borghi, N.; de Gennes, P.-G. *Langmuir* **2005**, *21*, 4144−4148.

(10) Odijk, T. *Macromolecules* **1983**, *16*, 1340−1344.

(11) Yang, Y.; Burkhardt, T. W.; Gompper, G. *Phys. Rev. E* **2007**, *76*, 011804.

(12) Odijk, T. *Phys. Rev. E* **2008**, *77*, 060901(R).

(13) Cifra, P.; Benková, Z.; Bleha, T. *J. Phys. Chem. B* **2009**, *113*, 1843−1851.

(14) Cifra, P. *J. Chem. Phys.* **2009**, *131*, 224903.

(15) Werner, E.; Persson, F.; Westerlund, F.; Tegenfeldt, J. O.; Mehling, B. *cond-mat.soft* 2012, arXiv:1201.2961v1201.

(16) Wagner, F.; Lattanzi, G.; Frey, E. *Phys. Rev. E* **2007**, *75*, 050902(R).

(17) Jun, S.; Thirumalai, D.; Ha, B.-Y. *Phys. Rev. Lett.* **2008**, *101*, 138101.

(18) Wang, Y.; Tree, D. R.; Dorfman, K. D. *Macromolecules* **2011**, *44*, 6594−6604.

(19) Jones, J. J.; van der Maarel, J. R. C.; Doyle, P. S. *Nano Lett.* **2011**, *11*, 5047−5053.

(20) Micheletti, C.; Marenduzzo, D.; Orlandini, E. *Phys. Rep.* **2011**, *504*, 1−73.

(21) Jung, Y.; Jeon, C.; Kim, J.; Jeoung, H.; Jun, S.; Ha, B.-Y. *Soft Matter* **2011**, DOI: 10.1039/c1031sm05706e.
(22) Semlyen, J. A. *Cyclic polymers*; Elsevier: London, 1986.
(23) Cifra, P. *J. Chem. Phys.* **2006**, *124*, 024706.
(24) Cifra, P.; Benková, Z.; Bleha, T. *J. Phys. Chem. B* **2008**, *112*, 1367−1375.
(25) Cifra, P.; Benková, Z.; Bleha, T. *Faraday Discuss.* **2008**, *139*, 377−392.
(26) Bulacu, M.; van der Giessen, E. *J. Chem. Phys.* **2005**, *123*, 114901.
(27) Rollins, G. C.; Petrov, A. S.; Harvey, S. C. *Biophys. J.* **2008**, *94*, L38−L40.
(28) Milchev, A.; Binder, K. *Macromolecules* **1996**, *29*, 343−354.
(29) Fynewever, H.; Yethiraj, A. *J. Chem. Phys.* **1998**, *108*, 1636−1644.
(30) Sheng, Y.-J.; Panagiotopoulos, S. K.; Kumar, S. K. *Macromolecules* **1996**, *29*, 4444−4446.
(31) Jang, S. S.; Çağin, T.; Goddard, W. A. *J. Chem. Phys.* **2003**, *119*, 1843−1854.
(32) Burkchard, W.; Schmidt, M. *Polymer* **1980**, *21*, 745−749.
(33) Cifra, P.; Bleha, T. *Polymer* **2007**, *48*, 2444−2452.
(34) Hsu, H.-P.; Paul, W.; Binder, K. *Macromolecules* **2010**, *43*, 3094−3102.
(35) Hsu, H.-P.; Paul, W.; Binder, K. *Europhys. Lett.* **2010**, *92*, 28003.
(36) Cifra, P.; Benková, Z.; Bleha, T. *Phys. Chem. Chem. Phys.* **2010**, *12*, 8934−8942.
(37) Ali, I.; Marenduzzo, D.; Yeomans, J. M. *Phys. Rev. Lett.* **2006**, *96*, 208102.
(38) Locker, C. R.; Harvey, S. C. *Multiscale Model. Simul.* **2006**, *5*, 1264−1279.
(39) Ali, I.; Marenduzzo, D.; Yeomans, J. M. *Biophys. J.* **2008**, *94*, 4159−4164.
(40) Skolnick, J.; Fixman, M. *Macromolecules* **1977**, *10*, 944−948.
(41) Odijk, T. *J. Polym. Sci., Part B: Polym. Phys* **1977**, *15*, 477−483.
(42) Teraoka, I.; Cifra, P.; Wang, Y. *Colloid. Surface. A* **2002**, *206*, 299−303.
(43) Dimitrov, D. I.; Milchev, A.; Binder, K.; Klushin, L. I.; Skvortsov, A. M. *J. Chem. Phys.* **2008**, *128*, 234902.
(44) Prentis, J. J. *J. Chem. Phys.* **1982**, *76*, 1574−1583.
(45) Robertson, R. M.; Laib, S.; Smith, D. E. *Proc. Natl. Acad. Sci. U.S.A.* **2006**, *103*, 7310−7314.
(46) Levy, S. L.; Mannion, J. T.; Cheng, J.; Reccius, C. H.; Craighead, H. G. *Nano Lett.* **2008**, *8*, 3839−3844.
(47) Burkhardt, T. W.; Yang, Y.; Gompper, G. *Phys. Rev. E* **2010**, *82*, 041801.
(48) Su, T.; Das, S. K.; Xiao, M.; Purohit, P. K. *PLoS ONE* **2011**, *6*, e16890.
(49) Köster, S.; Stark, H.; Pfohl, T.; Kierfeld, J. *Biophys. Rev. Lett* **2007**, *2*, 155−166.
(50) Dünweg, B.; Reith, D.; Steinhauser, M.; Kremer, K. *J. Chem. Phys.* **2002**, *117*, 914−924.
(51) Benková, Z.; Cifra, P. *Macromol. Theory Simul.* **2011**, *20*, 65−74.
(52) Sakaue, T.; Witz, G.; Dietler, G.; Wada, H. *Europhys. Lett.* **2010**, *91*, 68002.
(53) Dolgushev, M.; Berezovska, G.; Blumen, A. *J. Chem. Phys.* **2011**, *135*, 094901.
(54) Ostermeir, K.; Alim, K.; Frey, E. *Soft Matter* **2010**, *6*, 3467−3471.
(55) Köster, S.; Steinhauser, D.; Pfohl, T. *J. Phys.: Condens. Matter* **2005**, *17*, S4091−4104.
(56) Köster, S.; Kierfeld, J.; Pfohl, T. *Eur. Phys. J. E* **2008**, *25*, 439−449.
(57) Junier, I.; Martin, O.; Képès, F. *PLoS Comput. Biol.* **2010**, *6*, e1000678.
(58) Fritsche, M.; Heermann, D. W. *Soft Matter* **2011**, *7*, 6906−6913.
(59) Cifra, P.; Bleha, T. *Eur. Phys. J. E* **2010**, *32*, 273−279.
(60) Liu, Y.; Chakraborty, B. *Phys. Biol.* **2008**, *5*, 026004.